Effective dielectric modeling for antenna lenses using fill-factor analysis and the Nicolson–Ross–Weir method

Nguyen Duy Thai[1*], Hoang Van Phuc[2]

[1]Institute of Information Technology - Electronics, Academy of Military Science and Technology, 17 Hoang Sam, Nghia Do, Hanoi, Vietnam;
[2]Institute of System Integration, Le Quy Don Technical University, 236 Hoang Quoc Viet, Nghia Do, Hanoi, Vietnam.
[*]Corresponding author: ndthai03@gmail.com
Received 12 Mar. 2026; Revised 22 May 2026; Accepted 25 May 2026; Published 25 Jun. 2026.
DOI: https://doi.org/10.54939/1859-1043.j.mst.112.2026.73-82

ABSTRACT

The dielectric layer thickness is a key parameter in lens antenna systems, determining the controllability of phase distribution and radiation efficiency. However, the use of multiple materials with different dielectric constants often increases complexity and fabrication costs. To address this issue, this paper proposes establishing a streamlined and highly reliable design workflow for single-material lens antennas by rigorously validating a simple closed-form analytical method, based on the micro-periodic fill factor, against the complex Nicolson–Ross–Weir (NRW) parameter extraction algorithm. Computational and simulation results demonstrate that the effective dielectric values obtained from the analytical fill-factor approach exhibit excellent agreement with the NRW method, thereby proving that the proposed analytical model can effectively replace time-consuming full-wave parameter extraction processes and enable rapid optimization of the dielectric layer thickness. The method was applied to the design of a planar Lüneburg lens operating at 30 GHz, achieving an aperture efficiency above 0.9 across a broad frequency range while maintaining a stable beam pattern over various scanning angles. These results demonstrate the feasibility of the approach and highlight its potential for developing thin, easy-to-fabricate planar lens antennas suitable for high-frequency communication and radar systems.

Keywords: Antenna lens; Fill factor; Dielectric constant; Nicolson–Ross-Weir method.

1. INTRODUCTION

Antenna lenses are widely used in radio communication, radar, and high-frequency transmission systems due to their ability to transform wavefronts and generate narrow, high-gain beams. For dielectric lenses, controlling the phase distribution through the dielectric thickness is critical to focusing quality and radiation efficiency [1–5]. Conventional multilayer lenses achieve the desired phase response by combining materials with different dielectric constants, but this approach introduces significant design and fabrication challenges [6–9]. Gradient-index lenses such as the Lüneburg lens require multiple permittivity values, which increase manufacturing complexity and cost. Moreover, mismatched thermal expansion between layers can cause mechanical degradation, while assembly errors degrade radiation performance at millimeter-wave frequencies.

To overcome these limitations, this paper presents a design method that uses a single dielectric material with micro-periodic concentric ring structures. By varying the dielectric–air ratio, a continuous range of effective permittivity can be achieved without changing the base material [10–14]. This eliminates multi-material bonding interfaces, reduces fabrication tolerances, and lowers production costs. Accurate determination of effective permittivity is essential for such structures. The Nicolson–Ross–Weir (NRW) method provides reliable parameter extraction from S11 and S21 data, making it suitable for microstructured materials at millimeter-wave frequencies [15, 16]. Building on this, the main contribution of this paper is a streamlined design workflow for single-

material lens antennas. A newly derived analytical formulation for the fill factor is validated against the full-wave NRW method, showing strong agreement. This reduces reliance on iterative 3D simulations, minimizes computational overhead, and simplifies dielectric thickness optimization, enabling practical fabrication of thin, planar lens antennas for modern radar and communication systems.

2. PROPOSED METHOD FOR EFFECTIVE DIELECTRIC MODELING

2.1. Analytical fill-factor formulation for effective permittivity

In anisotropic media, the permittivity is no longer a scalar constant but is represented by a second-order tensor, which characterizes the directional dependence of the material properties in space. The relationship between the electric field E and the electric displacement D is expressed as: $D=\varepsilon \cdot E$. The permittivity tensor ε can be written in the form:

$$\varepsilon = \begin{bmatrix} \varepsilon_{xx} & \varepsilon_{xy} & \varepsilon_{xz} \\ \varepsilon_{yx} & \varepsilon_{yy} & \varepsilon_{yz} \\ \varepsilon_{zx} & \varepsilon_{zy} & \varepsilon_{zz} \end{bmatrix} \tag{1}$$

For a uniaxial anisotropic medium (with a single axis of symmetry), the permittivity tensor can be expressed as:

$$\varepsilon = \begin{bmatrix} \varepsilon_{\perp} & 0 & 0 \\ 0 & \varepsilon_{\perp} & 0 \\ 0 & 0 & \varepsilon_{\parallel} \end{bmatrix} \tag{2}$$

$\varepsilon_{\parallel}$ - is the permittivity corresponding to the component of the electric field E parallel to the axis of symmetry, $\varepsilon_{\perp}$ is the permittivity corresponding to the component of the electric field E perpendicular to the axis of symmetry. Consider a periodic medium composed of alternating planar layers of two isotropic dielectric materials, with a spatial period $d = a + b$, where a and b denote the thicknesses of the respective layers (Figure 1). Starting from Maxwell's equations for electromagnetic fields in a nonconductive medium (i.e., in the absence of free currents and sources):

$$\nabla^2 E - \mu\varepsilon \frac{\partial^2 E}{\partial t^2} = 0 \tag{3}$$

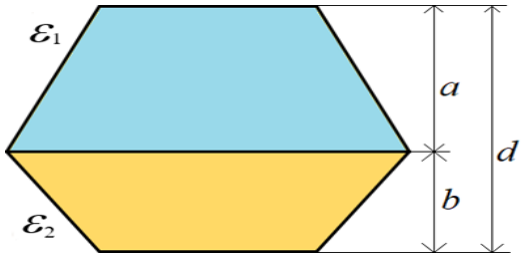

Figure 1. *Two adjacent dielectric layers forming a periodic unit cell.*

For a plane wave propagating along the y direction, the analysis is restricted to the E_y component. Assume a solution of the form:

$$E_y = u(z)e^{i\omega t} \tag{4}$$

where $u(z)$ denotes the spatially varying wave amplitude, $e^{i\omega t}$ represents the phase of the harmonic time oscillation. Applying the Helmholtz equation to the E_y field component yields:

$$\nabla^2 E_y - k^2 E_y = 0 \text{ with } k^2 = \mu\varepsilon\omega^2 \tag{5}$$

The Helmholtz equation can be further expanded as:

$$\frac{\partial^2 E_y}{\partial x^2} + \frac{\partial^2 E_y}{\partial z^2} + k^2 E_y = 0 \tag{6}$$

By employing the method of separation of variables, the solution is assumed to take the form:

$$E_y(x,z) = u(z)v(x) \tag{7}$$

By substituting (7) into (6), one obtains:

$$\frac{1}{v(x)}\frac{\partial^2 v(x)}{\partial x^2} + \frac{1}{u(z)}\frac{\partial^2 u(z)}{\partial z^2} + k^2 = 0 \tag{8}$$

The equation can be decomposed into two independent parts. Along the *x* direction is:

$$\frac{\partial^2 v(x)}{\partial x^2} + k_x{}^2 v(x) = 0 \tag{9}$$

By substituting (4) into (9), the resulting solution is obtained as:

$$v(x) = \exp(ik_x x) \tag{10}$$

Along the *z* direction:

$$\frac{\partial^2 u(z)}{\partial z^2} + k_z{}^2 u(z) = 0 \tag{11}$$

In a similar manner, the corresponding solution is obtained as: $u(z) = \exp(ik_z z)$. Consider the electromagnetic field behavior in a waveguide medium:

$$\begin{aligned} E_y(x,z) &= u(z)\exp(in(k_x x + k_z z)) \\ H_x(x,z) &= v(z)\exp(i(k_x x + k_z z)) \end{aligned} \tag{12}$$

where, $k_x = k_0 \cos\phi$, $k_z = k_0 \sin\phi$, ϕ – is the angle of incidence.

Substituting these expressions into Maxwell's equations yields a system of differential equations governing *u(z), v(z)*:

$$\frac{\partial^2 u_j}{\partial z^2} - 2ink_z \frac{\partial u_j}{\partial z} + k_0{}^2\left(\varepsilon_j \mu_j - n^2\right)u_j = 0 \tag{13}$$

$$v_j = \frac{-\left(i\frac{\partial u_j}{\partial z} + nk_z u_j\right)}{k_0 \mu_j} \tag{14}$$

The solution of the system of equations (10) and (11) results in

$$\begin{aligned} u_j &= A_j exp\left[iz\left(nk_z + \chi_j\right)\right] + B_j exp\left[iz\left(nk_z - \chi_j\right)\right] \\ v_j &= A_j \frac{\chi_j}{k_0 \mu_j} exp\left[iz\left(nk_z + \chi_j\right)\right] - B_j \frac{\chi_j}{k_0 \mu_j} exp\left[iz\left(nk_z - \chi_j\right)\right] \end{aligned} \tag{15}$$

with $\chi_j = \sqrt{k_0{}^2 \varepsilon_j \mu_j - k_x{}^2 n^2}$.

The coefficients A_j, B_j are determined from the continuity conditions of the E_y and H_x field components at the dielectric interfaces. By eliminating these coefficients, the final dispersion

equation is obtained as:

$$cos\left(k_z nd\right) = cos\left(\chi_1 a\right)cos\left(\chi_2 b\right) - \frac{1+\aleph^2}{2\aleph} \cdot sin\left(\chi_1 a\right)sin\left(\chi_2 b\right) \tag{16}$$

with $\aleph = \chi_1\mu_1 / \left(\chi_2\mu_2\right)$ and $a = cd$, where c is the filling factor.

2.2. Effective permittivity extraction via NRW algorithm

Determining the effective electromagnetic parameters of materials, particularly the refractive index n_d, is essential in the design of metamaterials, waveguides, antennas, and modern radar systems. For materials with complex internal structures or dimensions much smaller than the operating wavelength, direct measurement techniques are limited, motivating parameter extraction methods based on scattering data. Among these, the NRW method is one of the most widely used techniques [15], retrieving effective parameters from S11 and S21 measurements typically obtained with a vector network analyzer (VNA). The NRW method calculates the effective refractive index using a plane-wave propagation model through a finite-thickness sample. It is non-invasive, numerically stable, and applicable to a broad range of materials, including metamaterials with anomalous electromagnetic responses.

2.2.1. Principle of the Nicolson–Ross–Weir Method

Consider a planar sample of thickness a placed inside a waveguide or transmission line and illuminated by an incident electromagnetic wave. The VNA measurement provides two key quantities: the reflection coefficient S_{11} and the transmission coefficient S_{21}. These parameters contain information about the interaction between the electromagnetic wave and the sample, including reflection, attenuation, and phase effects. The NRW method is based on mapping the wave propagation problem through the material onto a one-dimensional transmission-line model. In this model, the sample is treated as a transmission-line section with an effective impedance and phase constant different from those of the surrounding medium. By analyzing the relationships among the incident, reflected, and transmitted waves, algebraic expressions can be derived that directly relate S_{11} to the effective refractive index and impedance. The configuration is illustrated in Figure 2.

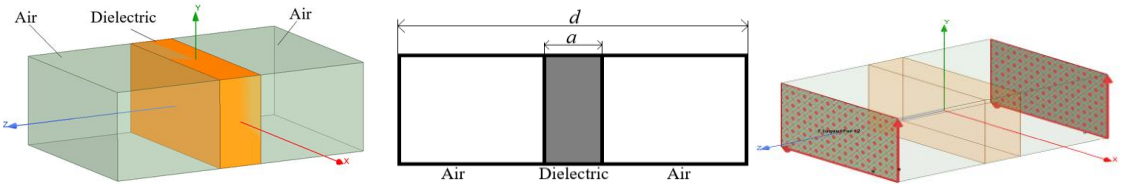

Figure 2. *Arrangement of the dielectric material and air within one period d: (a) 3D; (b) 2D view; c) Floquet ports 1 and 2.*

2.2.2. Unit cell model formulation

To perform the eigenmode analysis, the unit cell model is designed as a subwavelength periodic structure with a period d. Depending on the fabrication technique, the unit cell may take various forms, including a drilled-hole cylindrical cell, a square void structure, a dielectric post embedded in air, or a customized meta-atom configuration. The host material is characterized by a fixed dielectric constant ε_d while the air volume fraction is varied to obtain different filling-factor values.

$$D = \frac{V_{cell}}{V_{\text{air}}} \tag{17}$$

where V_{cell} – volume of the material, V_{air} – volume of the air.

To determine the effective refractive index of the periodic dielectric–air structure, full-wave electromagnetic simulations are performed using the finite element method in ANSYS HFSS. The unit cell is analytically defined with a fundamental period of $d = a + b$. However, to enforce structural symmetry required by the Floquet port boundaries, it is physically arranged as a one-dimensional dielectric stack ordered as $d=b/2+a+b/2$ maintaining the exact overall period d, where a denotes the thickness of the dielectric layer and b represents the air layer. Periodicity in the transverse direction is enforced by applying a pair of Master–Slave boundary conditions (Figure 2c), which allow a prescribed phase shift to be imposed between opposite faces of the unit cell.

2.2.3. Extraction of the effective dielectric constant

The NRW algorithm was developed based on solving a system of equations that describes plane-wave propagation. From the boundary conditions and the transmission-line model, the following expressions are obtained:

a) Relationship Between the Transmission Coefficient and the Reflection Coefficient

An important intermediate quantity is the reflection coefficient at the sample interface, denoted by Γ, which is derived from S_{11} and S_{21} through the following expression:

$$\Gamma = X \pm \sqrt{X^2 - 1} \tag{18}$$

where, $X = \dfrac{S_{11}^2 - S_{21}^2 + 1}{2S_{11}}$ (19)

The choice of the sign in the above expression is determined based on physical constraints to ensure that $|\Gamma| \leq 1$.

b) Extraction of the Effective Refractive Index

From the wave propagation model, the phase constant of the wave inside the material is described by: $e^{-in_d k_0 d} = X$ (20)

Accordingly, it is obtained that:

$$\begin{aligned} \ln(X) &= -in_d k_0 d \\ n_d &= \frac{1}{k_0 d}\left(i \ln(X)\right) \end{aligned} \tag{21}$$

The function $\ln(X)$ is multivalued:

$$\ln(X) = \ln|X| + i\left[\arg(X) + 2\pi m\right], \qquad m \in \mathbb{Z} \tag{22}$$

Therefore, the effective refractive index is determined by:

$$n_d = -\frac{1}{k_0 d}\left[(\arg(X) + 2\pi m - i \ln|X|\right], \qquad m \in \mathbb{Z} \tag{23}$$

2.3. Application to planar Lüneburg lens antenna design

A planar Luneburg lens, with a radially varying permittivity, enables the transformation of a planar wavefront into a converging wavefront focused at a fixed focal point:

$$n(r) = \sqrt{2 - \left(\frac{r}{R}\right)^2} \tag{24}$$

where R denotes the maximum radius of the circular lens., $0 \leq r \leq R$

The design parameters are chosen as follows: a period of $d = 2$ mm, an operating frequency of 30 GHz, dielectric permittivities $\varepsilon_d = \varepsilon_1 = 2.6$ (polystyrene), $\varepsilon_2 = 1$, and a lens radius of $R = 50$

mm. Using (16), the fill factor $c(r)$ is calculated, with the results presented in Figure 3. The lens structure is then formed by multiple concentric rings, where the physical thickness of each ring is directly determined by the obtained $c(r)$ values, as illustrated in Figure 4.

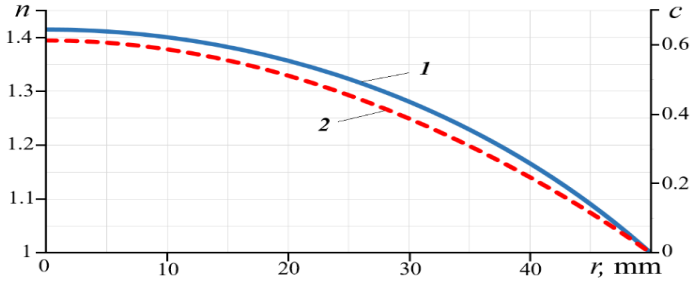

Figure 3. *Dependence of the permittivity and the filling factor on the radius: 1 – Permittivity; 2 – Filling factor.*

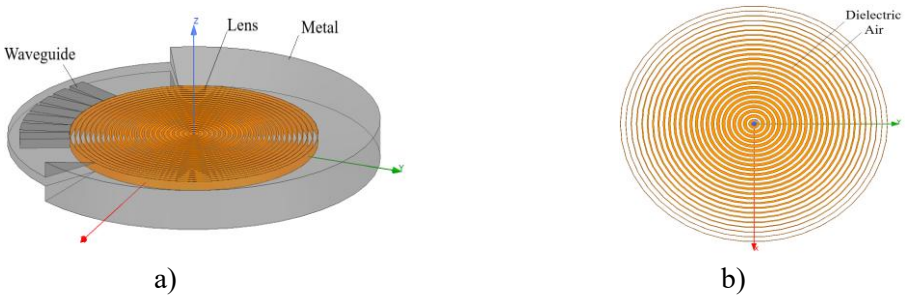

a) b)

Figure 4. *Structure of the planar concentric-ring Luneburg lens: (a) 3D view of the lens antenna; (b) Lens structure.*

3. VALIDATION AND PERFORMANCE EVALUATION

3.1. Comparative analysis of fill-factor and NRW methods

Consider the case where ϕ =0, under this condition $\varepsilon = \varepsilon_{||} = n^2$. To facilitate a comparison between the two methods, four different dielectric materials are considered: Teflon (ε=2.08), Polystyrene (ε=2.6), Megtron R5755(N) (ε=3.4), FR4 epoxy (ε=4.4). At an operating frequency of 30 GHz, the dielectric thickness is varied from 0 to 2 mm, with a unit cell size of d = 2 mm. Figure 5 presents the calculation results obtained using the fill-factor method (16) and the NRW method (23), illustrating the dependence of effective permittivity within one period d on dielectric layer thickness a for four dielectric materials. Across all materials, the effective permittivity increases monotonically with thickness, reflecting the greater proportion of dielectric in the micro-periodic structure. The characteristic curves from both methods are nearly identical over the entire thickness range, independent of substrate permittivity. Minor discrepancies appear only at larger thicknesses, attributable to higher-order scattering effects and limitations of the effective-medium model. These results confirm that the fill-factor method achieves high accuracy and can substitute for the NRW method in lens antenna design, particularly when rapid optimization and model simplification are required. Quantitative analysis from Figure 5 shows that the maximum relative deviation between the two methods remains very low: 0.3% for Teflon, 0.41% for Polystyrene, 0.76% for Megtron R5755(N), and 1.56% for FR4. Thus, the error consistently stays below 1.6%, even at larger thicknesses. This slight difference arises mainly from higher-order scattering effects fully captured in NRW simulations but simplified in the analytical model. Overall, the NRW method serves as a benchmark for physical accuracy, while the fill-factor method offers a practical design tool. Its simple analytical formulation eliminates the need for iterative 3D simulations,

enabling direct calculation and rapid optimization of single-material lens antenna designs with only minimal error.

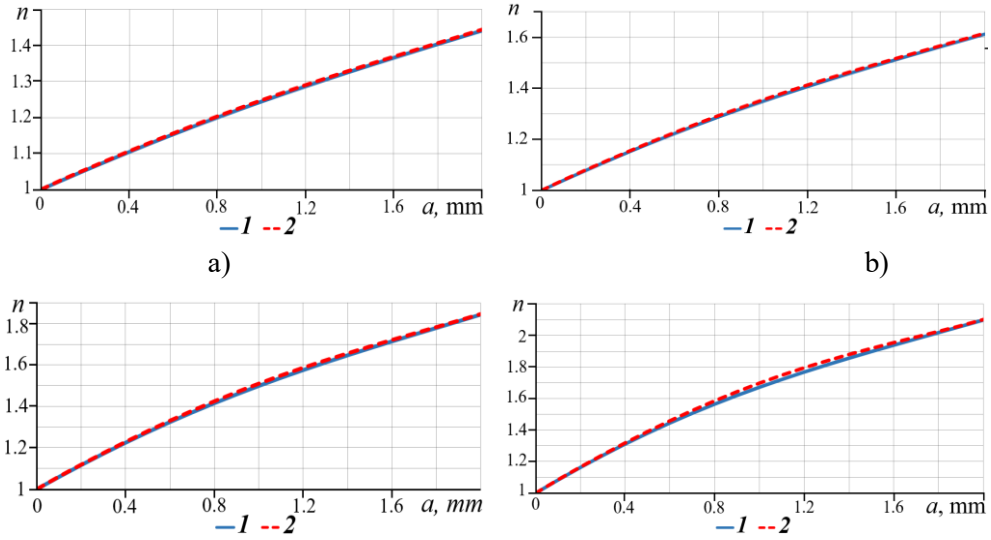

***Figure 5**. Dependence of the effective permittivity within one period d on the lens thickness a, calculated using method 1—the filling-factor method, and method 2—the NRW method, for different materials: (a) Teflon; (b) Polystyrene; (c) Megtron R5755(N); (d) FR4 epoxy.*

3.2. Full-wave verification of the planar Lüneburg lens antenna

Using the finite element method implemented in the Ansys HFSS antenna simulation software, the resulting electric field distribution illustrates the transformation of a cylindrical wavefront at the source into a planar wavefront at the lens output (Figure 6a).

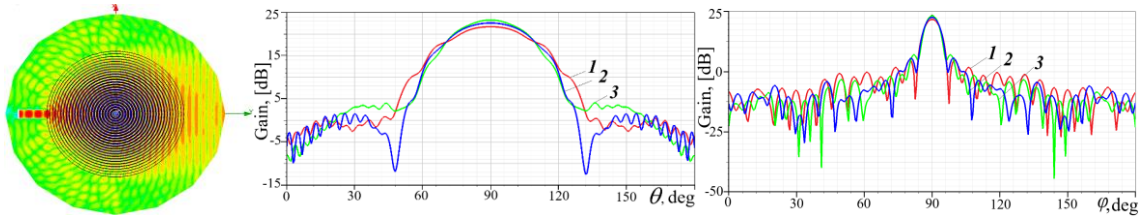

***Figure 6**. Radiation patterns of the antenna:*
a) Electric field distribution within the lens antenna; b).E-plane and c) H-plane.

The radiation patterns in the *E*- and *H*-planes at three different frequencies, 27, 30, and 33 GHz, are shown in Figure 6b,c. It can be observed that, at all three frequencies, the antenna exhibits a narrow main beam of approximately 6^0 and a sidelobe level of about −20 dB relative to the main lobe peak.

The antenna gain and aperture efficiency over the frequency range from 26 to 34 GHz are presented in Figure 7. Clearly, the antenna simulation yields very high performance, with an efficiency exceeding 0.9, indicating that the lens provides a uniform planar wavefront at the output.

Figure 8 presents the radiation patterns of the lens for different beam directions separated by 8^0. It can be observed that the beams exhibit nearly uniform gain and similar beamwidths, with narrow beams in the H-plane.

To highlight the advantages and practical value of the proposed method, Table 1 compares the

performance of the designed 30 GHz planar Luneburg lens with recently published lens antennas from 2024 and 2025 [17-19]. Recent advancements have focused on flat-bottom 3D printed geometries [17], axially tapered designs [18], or fully metallic implementations using transformation optics [19]. As observed in Table 1, while recent lenses achieve good performance, their aperture efficiencies are typically limited to the 71.3%–88.3% range [17, 18]. The metallic flat lens in [19] offers robust structural properties but suffers from a lower peak efficiency of 65%. In contrast, the proposed planar design utilizes a straightforward single-material fill-factor analytical approach. Despite its simplicity, it operates over a wide fractional bandwidth (26–34 GHz) and yields a highly competitive maximum gain of approximately 24 dB. Most notably, it achieves an outstanding aperture efficiency exceeding 0.9 (90%), validating that the exact fill-factor optimization method provides precise phase control that is superior to several complex configurations.

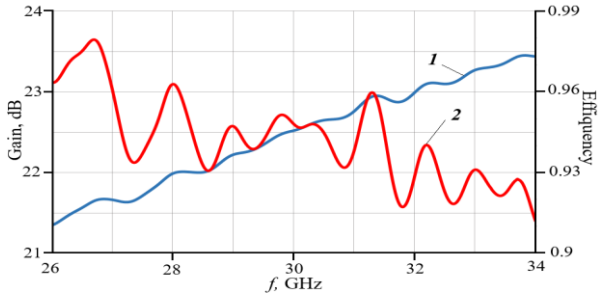

Figure 7. *Frequency dependence of the antenna gain and aperture efficiency: 1- Gain, 2 – Aperture efficiency.*

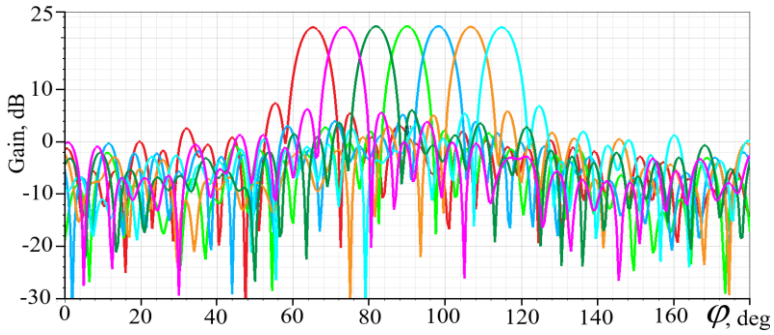

Figure 8. *Radiation patterns of the lens antenna with seven beams steered at 8^0 intervals for $\theta = 90^0$*

Table 1. *Comparison of the proposed lens antenna with other recent works.*

Reference / year	**Lens type**	**Frequency band**	**Material strategy**	**Max gain (dB / dBi)**	**Peak aperture efficiency (%)**
[17]/2025	Flat-bottom LL	14.1 GHz (Ku-band)	3D printed/ transformation optics	17.7	71.3%
[18]/2025	Planar LL	W-band	3D printed/ index tapering	21.8	88.3%
[19]/2024	Flat metallic LL	35–45 GHz	Fully metallic	15.8	65.0%
Proposed	**Planar Luneburg lens**	**26 – 34 GHz**	**Single-material (fill-factor)**	**~24.0**	**> 90.0%**

In practical engineering implementations, physical constraints limit the aperture efficiency.

Continuous wave impedance mismatches at the concentric ring interfaces generate parasitic reflections, which degrade the impedance matching across the lens surface. Although the progressive gradient profile minimizes these localized boundary reflections, a part of the electromagnetic energy reflects backward instead of focusing. Additionally, mechanical fabrication tolerances from CNC milling or additive manufacturing cause structural variations in the physical dimensions of the micro-periodic rings. These geometric deviations change the localized filling factor, introducing phase errors across the aperture surface. These non-ideal mechanisms reduce the physical aperture efficiency by 5% to 8% in hardware compared to the software models.

4. CONCLUSIONS

This paper has presented an efficient method for determining the dielectric layer thickness in a lens antenna structure using only a single dielectric material. By combining the filling-factor approach with the effective electromagnetic parameter extraction method based on the NRW algorithm, a highly accurate and practically implementable model for evaluating the effective permittivity has been developed. The comparison between the two methods demonstrated that the maximum deviation of less than 1.6% over the investigated thickness range approves the reliability of the filling-factor model in simulating the phase response and tuning the effective permittivity of micro-periodic structures. This simplifies the optimization process and reduces computational overhead in lens antenna problems. The proposed method has been successfully applied to the design of a planar Luneburg lens operating at 30 GHz. Full-wave electromagnetic simulations demonstrate that the lens achieves an aperture efficiency greater than 0.9 over a wide frequency band from 26 to 34 GHz, while maintaining stable gain and uniform beam characteristics across multiple steering angles. Future research will focus on the fabrication of lens prototypes using 3D printing technology and experimental verification with VNA measurements to fully validate the proposed design workflow. These experimental results will provide further insights into the practical performance and manufacturing tolerances of the single-material lens antenna. Furthermore, the proposed methodology can be extended to meta-lens structures, three-dimensional gradient-index lenses, and antenna systems operating in millimeter-wave or terahertz frequencies, where stringent phase accuracy and material design flexibility are required.

REFERENCES

[1]. Зелкин Е.Г., Петрова Р.А. *"Линзовые антенны"*. М.: Сов. радио, (1974).

[2]. John Thornton & Kao-Cheng Huang. *"Modern Lens Antennas for Communications Engineering"*. Wiley-VCH, (2013).

[3]. C. A. Fernandes, E. B. Lima, J. R. Costa. *"Dielectric Lens Antennas, in Handbook of Antenna Technologies"*. Springer Singapore, (2015).

[4]. Milne R. *"Dipole array lens antenna"*. IEEE Trans Antennas and Propagation, pp. 704-712, (1982). DOI: 10.1109/TAP.1982.1142835.

[5]. Guo Y.J., Ansari M., Ziolkowski R.W., Fonseca N.J.G. *"Quasi-optical multi-beam antenna technologies for B5G and 6G mmwave and THz networks: A review"*. IEEE Open J Antennas Propag, 2, pp. 807-830, (2021). DOI: 10.1109/OJAP.2021.3093622.

[6]. Luneburg R.K. *"Mathematical Theory of Optics"*. Providence: Brown Univ., (1944).

[7]. Henry Giddens, Yang Hao. *"Multi-Beam Graded Dielectric Lens Antenna from Multi-Material 3D Printing"*. arXiv preprint, (2020).

[8]. Dhouibi A., Burokur S.N., de Lustrac A., Priou A. *"Low-profile substrate-integrated lens antenna using metamaterials"*. IEEE Antennas Wirel Propag Lett, 12, pp. 43-46, (2013). DOI: 10.1109/LAWP.2012.2237372.

[9]. Li Q.L., Cheung S.W., Wu D., Yuk T.I. *"Microwave lens using periodic dielectric sheets for antenna-gain enhancement"*. IEEE Trans Antennas and Propagation, 65, (4), pp. 2068-2073, (2017). DOI: 10.1109/TAP.2017.2670441.

[10]. Khaled Aljaloud, Yosef T Aladadi, Majeed A S Alkanhal, Wazie M Abdulkawi, Rifaqat Hussain. *"A Wideband GRIN Dielectric Lens Antenna for 5G Applications"*. Micromachines (Basel), (2023).
[11]. Zhao L.-W., Wu Y.F., Wang C., Guo Y. *"A 3-D-printed deployable luneburg lens antenna based on the pop-up kirigami sphere"*. IEEE Trans Antennas and Propagation, 71, (8), pp. 6481-6489, (2023). DOI: 10.1109/TAP.2023.3288548.
[12]. Trzebiatowki K., Kalista W., Rzymowski M., Kulas L., Nyka K. *"Multibeam antenna for Ka-band CubeSat connectivity using 3-D printed lens and antenna array"*. IEEE Antennas Wirel Propag Lett, 21, (11), pp. 2244-2248, (2022). DOI: 10.1109/LAWP.2022.3189073.
[13]. Monkevich. M., Le Sage G.P. *"Design and fabrication of a custom-dielectric fresnel multi-zone plate lens antenna using additive manufacturing techniques"*. IEEE Access, 7, pp. 61452-61460, (2019). DOI: 10.1109/ACCESS.2019.2916077.
[14]. Giddens H., Andy A.S., Hao Y. *"Multimaterial 3-D printed compressed luneburg lens for mm-wave beam steering"*. IEEE Antennas Wirel Propag Lett, 20, (11), pp. 2166-2170, (2021). DOI: 10.1109/LAWP.2021.3109591.
[15]. Edward J. Rothwell et al. *"Analysis of the Nicolson-Ross-Weir Method for Characterizing the Electromagnetic Properties of Engineered Materials"*. (2016).
[16]. G. Angiulli & M. Versaci. *"Extraction of the Electromagnetic Parameters of a Metamaterial Using the Nicolson–Ross–Weir Method"*. Applied Sciences, (2022).
[17]. Guo-Ting Liang, Bo-Hai Zhang, Shuai Gao. *"A Luneburg Lens Antenna with High Aperture Efficiency"*. 2025 International Symposium on Antennas and Propagation (ISAP), (2025).
[18]. Nannan Wang, Yizhi Zhang, Jingjing Liu. *"A 3D-Printed Planar Luneburg Lens with Beam Enhancement via Axially Added Refractive Index Tapering"*. 2025 International Symposium on Antennas and Propagation (ISAP), (2025).
[19]. Kunning Liu, Jingbo Zhou, Liang Li. *"Flat Fully Metallic Luneburg Lens Antenna for Millimeter-Wave Communication"*. 2024 IEEE International Symposium on Antennas and Propagation, (2024).

TÓM TẮT

Mô hình hóa điện môi hiệu dụng cho thấu kính ăng ten sử dụng phân tích hệ số lấp đầy và phương pháp Nicolson–Ross–Weir

Độ dày lớp điện môi là một tham số quan trọng trong hệ thống ăng ten thấu kính, quyết định khả năng kiểm soát phân bố pha và hiệu suất bức xạ. Tuy nhiên, việc sử dụng nhiều vật liệu với hằng số điện môi khác nhau thường làm tăng độ phức tạp và chi phí chế tạo. Để giải quyết vấn đề này, bài báo đề xuất một quy trình thiết kế đơn giản và đáng tin cậy cho ăng ten thấu kính sử dụng một loại vật liệu dựa trên kiểm chứng theo phương pháp phân tích hệ số lấp đầy vi tuần hoàn, so sánh với thuật toán trích xuất tham số Nicolson–Ross–Weir (NRW) phức tạp. Kết quả tính toán và mô phỏng cho thấy giá trị điện môi hiệu dụng thu được từ phương pháp hệ số lấp đầy có sự tương đồng cao với phương pháp NRW, qua đó chứng minh mô hình phân tích đề xuất có thể thay thế hiệu quả cho các quy trình trích xuất tham số toàn sóng và cho phép tối ưu nhanh độ dày lớp điện môi. Phương pháp này đã được áp dụng để thiết kế thấu kính phẳng Lüneburg hoạt động ở tần số 30 GHz, đạt hiệu suất khẩu độ trên 0,9 trong một dải tần rộng đồng thời duy trì dạng búp sóng ổn định ở nhiều góc quét khác nhau. Những kết quả này khẳng định tính khả thi của phương pháp và cho thấy tiềm năng ứng dụng trong việc phát triển các anten thấu kính phẳng mỏng, dễ chế tạo, phù hợp cho hệ thống thông tin và radar tần số cao.

Từ khoá: Thấu kính ăng ten; Hệ số lấp đầy; Hằng số điện môi; Phương pháp Nicolson–Ross–Weir.